A Central Role of RLIP76 in Regulation of Glycemic Control

Sanjay Awasthi, Sharad S. Singhal, Sushma Yadav, Jyotsana Singhal, Rit Vatsyayan, Ewa Zajac, Rafal Luchowski, Jozef Borvak, Karol Gryczynski, and Yogesh C. Awasthi

OBJECTIVE—Pathology associated with oxidative stress frequently results in insulin resistance. Glutathione (GSH) and GSH-linked metabolism is a primary defense against oxidative stress. Electrophilic lipid alkenals, such as 4-hydroxy-*t*-2-nonenal (4HNE), generated during oxidative stress are metabolized primarily to glutathione electrophile (GS-E) conjugates. Recent studies show that RLIP76 is the primary GS-E conjugate transporter in cells, and a regulator of oxidative-stress response. Because RLIP76$^{-/-}$ mice are hypoglycemic, we studied the role of RLIP76 in insulin resistance.

RESEARCH DESIGN AND METHODS—Blood glucose, insulin, lipid measurements, and hyperinsulinemic-euglycemic and hyperglycemic clamp experiments were performed in RLIP76$^{+/+}$ and RLIP76$^{-/-}$ C57B mice, using Institutional Animal Care and Use Committee–approved protocols. Time-resolved three-dimensional confocal fluorescence microscopy was used to study insulin endocytosis.

RESULTS—The plasma insulin/glucose ratio was ordered RLIP76$^{-/-}$ < RLIP76$^{+/-}$ < RLIP76$^{+/+}$; administration of purified RLIP76 in proteoliposomes to RLIP76$^{+/+}$ animals further increased this ratio. RLIP76 was induced by oxidative or hyperglycemic stress; the concomitant increase in insulin endocytosis was completely abrogated by inhibiting the transport activity of RLIP76. Hydrocortisone could transiently correct hypoglycemia in RLIP76$^{-/-}$ animals, despite inhibited activity of key glucocorticoid-regulated hepatic gluconeogenic enzymes, phosphoenolpyruvate carboxykinase, glucose-6-phosphatase, and fructose 1,6-bisphosphatase, in RLIP76$^{-/-}$.

CONCLUSIONS—The GS-E conjugate transport activity of RLIP76 mediates insulin resistance by enhancing the rate of clathrin-dependent endocytosis of insulin. Because RLIP76 is induced by oxidative stress, it could play a role in insulin resistance seen in pathological conditions characterized by increased oxidative stress. ***Diabetes*** **59:714–725, 2010**

Oxidative stress is implicated in chronic diseases (1–4) including insulin resistance that leads to type 2 diabetes (5–8). Pancreatic β-cells are relatively susceptible to the damaging effects of free radicals because of low levels of free radical quenching enzymes including catalase, glutathione peroxidase, and superoxide dismutase (9). Short exposure of β-cells to H_2O_2 suppresses insulin mRNA levels and insulin secretion (10). Likewise, exposure of β-cells to high glucose concentrations leads to increased intracellular free radical content and inhibited insulin release (11). Reactive oxygen species (ROS) generated during oxidative stress are known to activate signaling proteins including stress kinases (e.g., c-Jun NH_2-terminal kinase, p38, inhibitor of κB kinase) in addition to the extracellular receptor kinases that can affect the cellular response to insulin. The down-regulation of insulin response under oxidant exposure involves activation of tumor necrosis factor-α; increased Ser/Thr phosphorylation of insulin receptor and insulin receptor substrate-1 (IRS1) (12,13) reduces the redistribution of IRS1 and phosphatidylinositol 3 kinase from the cytosolic to microsomal fraction, reduces protein kinase-B (Akt) phosphorylation, and results in decreased trafficking of GLUT4 to the plasma membrane. Prolonged exposure to oxidative stress also affects the transcription of GLUT4 (14).

In parallel with the protein signaling pathway described above, a chemical signaling pathway is activated by oxidative stress. This pathway begins with ROSs derived from oxidative degradation of polyunsaturated fatty acids, and is linked with multiple protein signaling pathways. Activation of protein kinase C and nuclear factor-κB results in increased activity of NADPH oxidase (15), which amplifies oxidative stress by augmenting the recycling of Fe^{3+} to Fe^{2+} (16). The autocatalytic chain reaction of lipid peroxidation, where a single lipid peroxide species can lead to the formation of up to a thousand lipid peroxides, provides a built-in magnification for ROS-mediated signaling. The α- and β-unsaturated lipid aldehydes generated through β-scission of linoleic acid, γ-linoleic acid, or arachidonic acid hydroperoxides play an important role in this signaling. 4-Hydroxy-*t*-2-nonenal (4HNE), the most abundant alkenal generated in cells, is a versatile second messenger for signaling that can affect multiple signaling pathways including those for apoptosis, differentiation, proliferation, and receptor tyrosine-kinase (RTK)–mediated signaling (17,18).

4HNE controls the expression and activity of many signaling proteins involved in insulin resistance, including stress kinases, nuclear factor-κB, and chaperones (19), and affects RTK signaling, thus HNE could modulate insulin signaling and glucose homeostasis. Glutathione transferases (particularly GSTA4–4) and RLIP76 (a 76-kDa splice variant, encoded by the human gene *RALBP1*) are the two major determinants of 4HNE levels in cells (20). Although 4HNE is substrate for several enzymes including aldehyde dehydrogenases, aldose reductase, and Cyt-p450, the major pathway for its disposition from cells is through its GST catalyzed conjugation to GSH (20) and subsequent ATP-dependent transport of the conjugate (GS-HNE) catalyzed by RLIP76 (21). The mechanisms for the efflux of

From the Department of Molecular Biology & Immunology, University of North Texas Health Science Center, Fort Worth, Texas.
Corresponding author: Sanjay Awasthi, sawasthi@hsc.unt.edu.
Received 19 June 2009 and accepted 25 November 2009. Published ahead of print at http://diabetes.diabetesjournals.org on 10 December 2009. DOI: 10.2337/db09-0911.

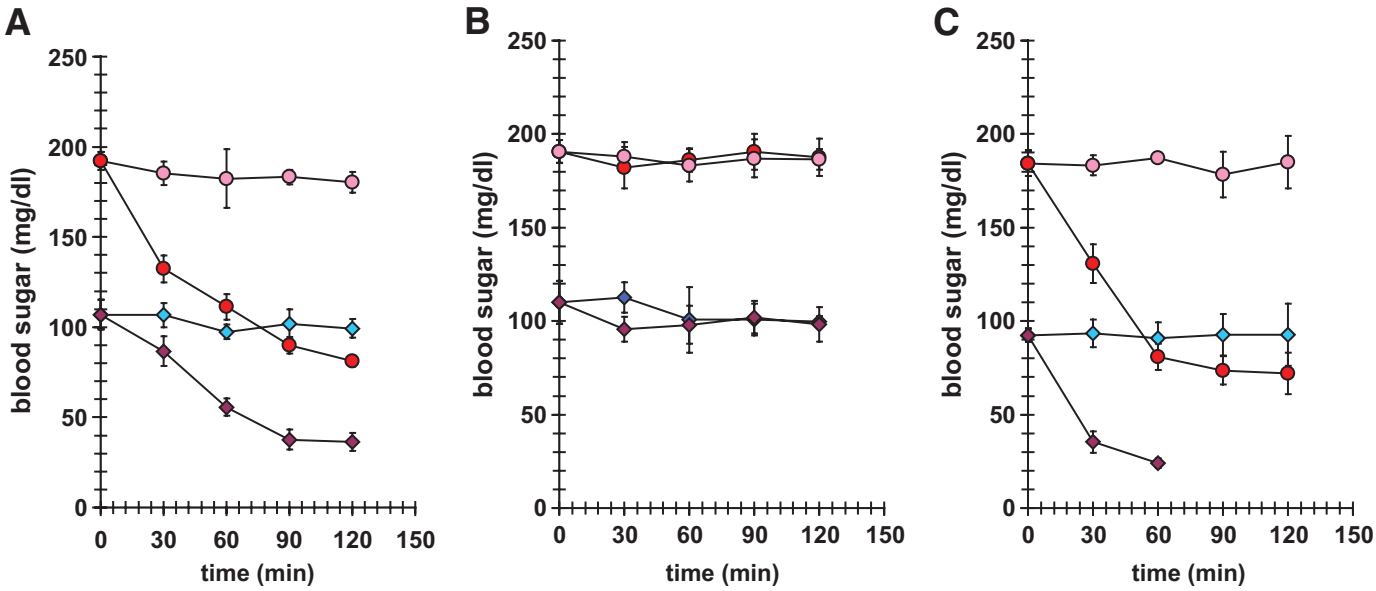

FIG. 1. Effect of intraperitoneal administration of insulin on blood glucose in RLIP76$^{+/+}$ vs. RLIP76$^{-/-}$ animals. Level of blood glucose at 2 h (*A*) and 24 h (*B*) after a single dose of insulin administered intraperitoneally. At readministration of insulin on day 2, the RLIP76$^{+/+}$ blood glucose level goes down. The insulin sensitivity of RLIP76$^{-/-}$ was magnified significantly, with death of all animals before 90 min (*C*). Blood glucose at the time of death was undetectable. RLIP76$^{+/+}$, ●; RLIP76$^{-/-}$, ◇. Pink and blue indicate no insulin; red and purple indicate insulin dosing.

glutathione electrophile (GS-E) conjugates are complex, involving other ABC transporters, but knockout mouse studies have shown that RLIP76 plays a dominant role (22,23). The relevance of RLIP76 to insulin resistance is also suggested by its known function as a component of clathrin-dependent endocytosis (22–26), a determinant of the duration of ligand-receptor signal. Present studies provide evidence for a novel model in which the mechanisms of insulin resistance are directly linked to mercapturic acid pathway through the role of RLIP76 as an energy-providing component of clathrin-dependent endocytosis. Compelling evidence for this model is presented in this communication.

RESEARCH DESIGN AND METHODS

Quantification of insulin, glucose, and lipid levels in wild-type and RLIP76 knockout mice. Animal experiments were carried out in accordance with an Institutional Animal Care and Use Committee (IACUC)–approved protocol. Twelve-week-old C57BL/6 mice born of heterozygous × heterozygous (RLIP76$^{+/-}$ × RLIP76$^{+/-}$) mating were genotyped by PCR strategy on mouse tail DNA using forward, reverse, and long terminal region primers (27). Insulin and glucose measurement in blood serum was performed on wild-type (RLIP76$^{+/+}$) animals killed 24 h after a single intraperitoneal injection of control or RLIP76 liposomes equivalent to 200 and 500 μg RLIP76 protein. Insulin and glucose measurement in blood serum was also performed on heterozygous (RLIP76$^{+/-}$) and homozygous (RLIP76$^{-/-}$) animals. Cholesterol, triglycerides, glucose, and insulin measurements were reassayed and verified in the laboratory of Dr. Kent R. Refsal, Michigan State University, East Lansing, Michigan. Uptake of RLIP76 by tissues of RLIP76 proteoliposome–injected mice was monitored by comparing the results of Western blots of tissues of wild-type mice with or without administration of RLIP76 proteoliposomes.

Hyperinsulinemic-euglycemic and hyperglycemic clamp experiments. Hyperinsulinemic-euglycemic and hyperglycemic clamp experiments were performed by the Mouse Metabolic Phenotyping Center at the Yale University School of Medicine, with procedures approved by Yale University Institutional Animal Care and Use Committee. Briefly, RLIP76$^{+/+}$ and RLIP76$^{-/-}$ mice were anesthetized with an intraperitoneal injection of ketamine and xylazine, a catheter was inserted in the right jugular vein, a 3-way connector was attached to the jugular vein catheter for intravenous infusion, and blood samples were obtained from tail vessels, requiring a small tail cut. A 2-h hyperinsulinemic-euglycemic clamp was conducted with a primed-continuous infusion of human insulin at a rate of 15 pmol · kg^{-1} · min^{-1} to raise plasma insulin within a physiological range (~300 pmol/l). Blood samples were collected at 10- to 20-min intervals for the immediate measurement of plasma glucose concentration, and 20% glucose was infused at variable rates to maintain glucose at basal concentrations (~6 mmol/l). Insulin-stimulated whole-body glucose metabolism was assessed with a continuous infusion of 3-[^{3}H] glucose (0.1 mCi/min) throughout the clamps. Basal rates of whole-body glucose turnover were assessed using a primed-continuous infusion of 3-[^{3}H] glucose for 2 h prior to the start of clamp. To estimate insulin-stimulated glucose uptake in individual tissues, 2-deoxy-D-1-[^{14}C] glucose (2-[^{14}C] DG) is administered as a bolus (10 mCi) at 75 min after the start of clamp. Blood samples were taken at 0–120 min of clamp for the measurement of plasma 3-[^{3}H] glucose and/or 2-[^{14}C] DG concentrations. Additional blood samples were collected before and at the end of clamp for the measurement of plasma insulin concentrations. A 2-h hyperglycemic clamp is conducted with a variable infusion of 20% glucose to raise and maintain plasma glucose concentrations at ~16 mmol/l. Blood samples were collected at 10- to 20-min intervals for the immediate measurement of plasma glucose concentrations using Beckman Glucose Analyzer. The area under curve of plasma glucose and insulin profiles was assessed to determine glucose-induced insulin secretion in vivo (28).

Phosphoenolpyruvate carboxykinase, fructose 1,6-bisphosphatase, and glucose-6-phosphatase activity in wild-type and RLIP76 knockout mice. The method of Opie and Newsholme (29) was used for phosphoenolpyruvate carboxykinase (PEPCK) assay. Fructose 1,6-bisphosphatase (F-1,6-BPase) was assayed by the method of Taketa and Pogell (30). Glucose-6-phosphatase (G6Pase) activity was determined using the method of Gierow and Jergil (31). Expression of *PEPCK*, *F-1,6-BPase*, and *G6Pase* genes in wild-type (RLIP76$^{+/+}$) and RLIP76 knockout (RLIP76$^{-/-}$) mouse liver tissues was also quantitated by RT-PCR analysis using QIAGEN one-step RT-PCR kit following manufacturer's instructions. Briefly, liver tissues were placed in RNAlater reagent and RNA was isolated using RNeasy tissue kit (QIAGEN) and was quantified; purity was determined by measuring absorbance at 260 and 280 nm. All primers were designed to have a melting temperature of 60 ± 5°C. Gene-specific primers (PEPCK: upstream primer 5′ GAGTATATCCACATCTGC GATGGC and reverse primer 5′ GGCGAGTCTGTCAGTTCAATACCAATC, yielding 400-bp product; F-1,6-BPase: upstream primer 5′GCTCAACTCGAT GCTGACTGCC and reverse primer 5′ ACCAGGGTTCGACTACCATACAGTG, yielding 350-bp product; G6Pase: upstream primer 5′AGCTGTGGGCATTA AACTCC and downstream primer 5′ AATGCCTGACAGGACTCCAG, yielding the product of 400 bp) were used for RT-PCR. The RT-PCR product was run on 1% agarose gel and bands were quantified using AlphaImager HP (Alpha Innotech, San Leandro, CA). β-Actin was used as an internal control.

Fluorescein isothiocyanate-conjugated insulin binding and internalization assay. RLIP76 mouse embryonic fibroblasts (MEFs; 0.1 × 10^6 cells/ml) were grown on sterilized glass coverslips (18-mm size) in RPMI-1640 medium

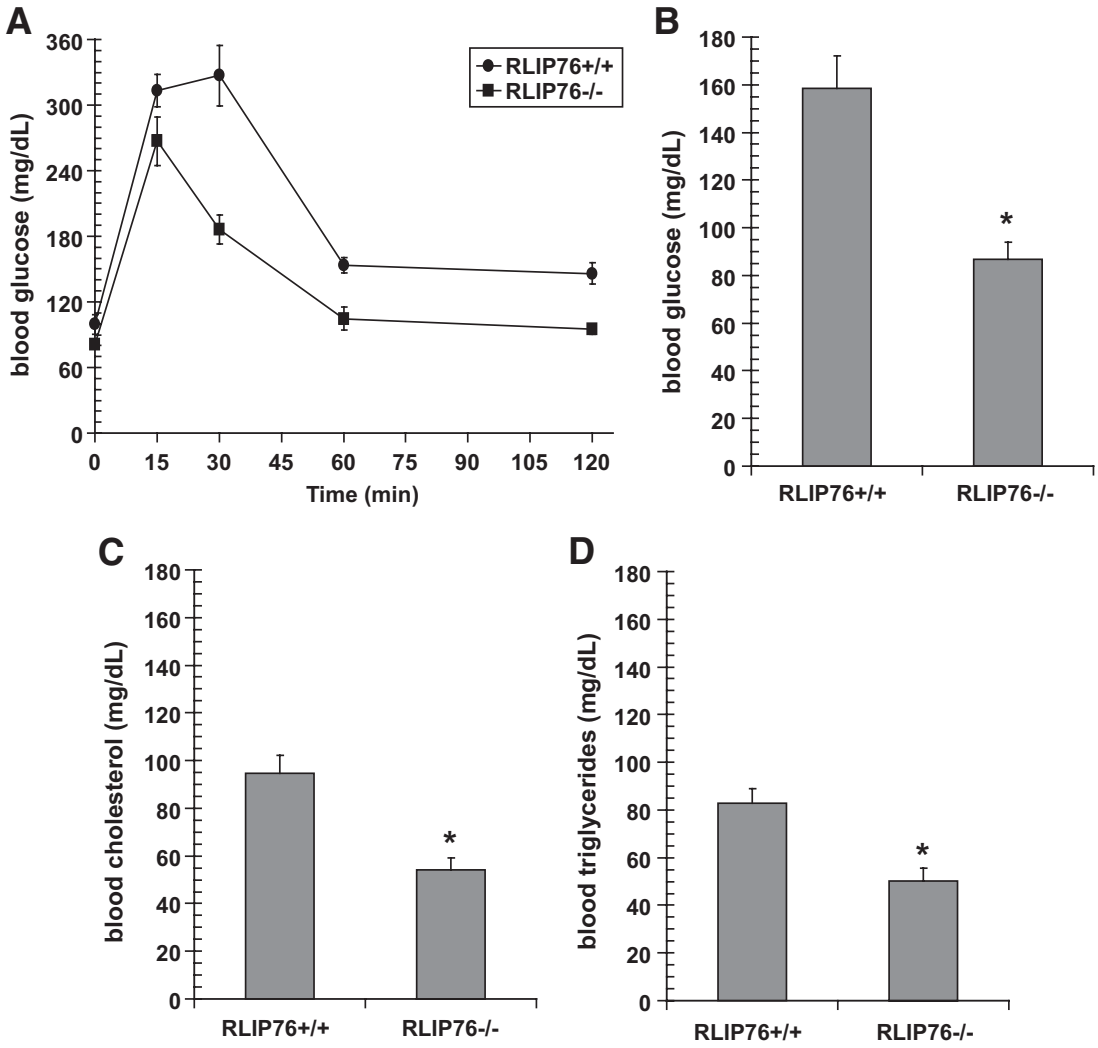

FIG. 2. Glucose tolerance test and lipid levels in RLIP76$^{-/-}$ mice. For the glucose tolerance test, C57B mice (wild-type and RLIP76$^{-/-}$) were fasted for 6 h followed by oral administration of 2 *g*/kg body wt glucose using a gavage needle. Each of five groups consisted of five animals each. One group was killed at each time point (0, 5, 30, 60, and 120 min) and ~200–300 μl of blood was sampled for glucose analyses. Blood was kept refrigerated for ~4 h and centrifuged at 3,000*g* for 10 min, and the serum was separated and stored at −20°C until assay. Glucose, cholesterol, and triglycerides measurement was performed in the laboratory of Dr. Kent R. Refsal, Michigan State University. *Statistical analyses by ANOVA were significant at $P < 0.001$ for RLIP76$^{-/-}$ vs. RLIP76$^{+/+}$ animals; $n = 5$.

in tissue culture–treated 12-well plates overnight, followed by washing with PBS. Cells were incubated with 100 ng/ml fluorescein isothiocyanate (FITC)–conjugated insulin (prepared in PBS containing 1% BSA) for 60 min in ice (4°C). Cells were then incubated at 37°C in humidified chamber for 10 min followed by fixation with 4% paraformaldehyde. Slides were analyzed using confocal laser scanning microscopy with Zeiss 510 meta system (Carl Zeiss, Jena, Germany), with excitation at 555 nm and emission at 580 nm.

Preparation and application of insulin-quantum dot. Insulin-quantum dot (QD) complexes were formed by incubation of insulin (100 nmol/l; Life Technologies) with QDs 605 ITK (Molecular Probes) at 4°C with mixing for 30 min. A molar ratio of 6:1 of insulin:QDs was used. To remove unbound ligand, the complexes were purified by chromatography over P30 size-exclusion spin columns (Bio-Rad, Hercules, CA).

Transfection of RLIP76$^{-/-}$ MEFs with RLIP76-pEGFP-C1 vector and insulin-QD labeling. RLIP76$^{-/-}$ MEFs were transiently transfected with pEGFP-C1 vector alone or with RLIP76-pEGFP-C1 vector using Lipofectamine 2000 (Invitrogen, Carlsbad, CA). RLIP76$^{-/-}$ control and RLIP76$^{-/-}$-transfected MEFs (0.1×10^6) were grown on sterilized glass coverslips in RPMI-1640 medium in tissue culture–treated 12-well plates overnight. Cells were labeled with insulin:QD for 45 min at 4°C, washed with PBS, incubated for 10 min at 37°C, and fixed in 4% paraformaldehyde. Slides were analyzed by confocal laser scanning microscopy with Zeiss 510 meta system (excitation 594/emission 610 for insulin:QD and excitation 488/emission 507 nm for GFP-RLIP76).

Förster resonance energy transfer analysis. RLIP76$^{-/-}$ MEFs were transiently transfected with pEGFP-C1 vector alone or with RLIP76-pEGFP-C1 vector using Lipofectamine 2000 (Invitrogen). Transfection efficiency was measured by fluorescent microscope (excitation/emission 488/507 nm), and RLIP76 mRNA expression was evaluated by RT-PCR analysis. RLIP76$^{-/-}$ control and RLIP76$^{-/-}$-transfected MEFs (1×10^5) were grown on sterilized glass coverslips in RPMI-1640 medium in 12-well plates overnight and were treated with 10 μmol/l doxorubicin (DOX) or 10 μmol/l glutathione-monochlorobimane for 20 min at 37°C, washed with PBS, and fixed in 4% paraformaldehyde. Molecular interactions were visualized by Förster resonance energy transfer (FRET) as described (32).

Statistical methods. All data were evaluated with a two-tailed unpaired Student *t* test or compared by one-way ANOVA and are expressed as means ± SD. A value of $P < 0.05$ was considered statistically significant.

RESULTS

RLIP76 gene interruption causes hypoglycemia and apparent insulin sensitivity. The baseline blood glucose in RLIP76$^{-/-}$ mice was 46% lower than in RLIP76$^{+/+}$ animals ($P < 0.001$). At 2 h after insulin injection, blood glucose dropped by 55% in RLIP76$^{+/+}$ versus 67% in RLIP76$^{-/-}$ ($P < 0.01$) (Fig. 1*A*). At 24 h after insulin injection (Fig. 1*B*), blood glucose levels had returned to baseline in all animals. The RLIP76$^{+/+}$ had quantitatively a very similar response to readministration of insulin on day

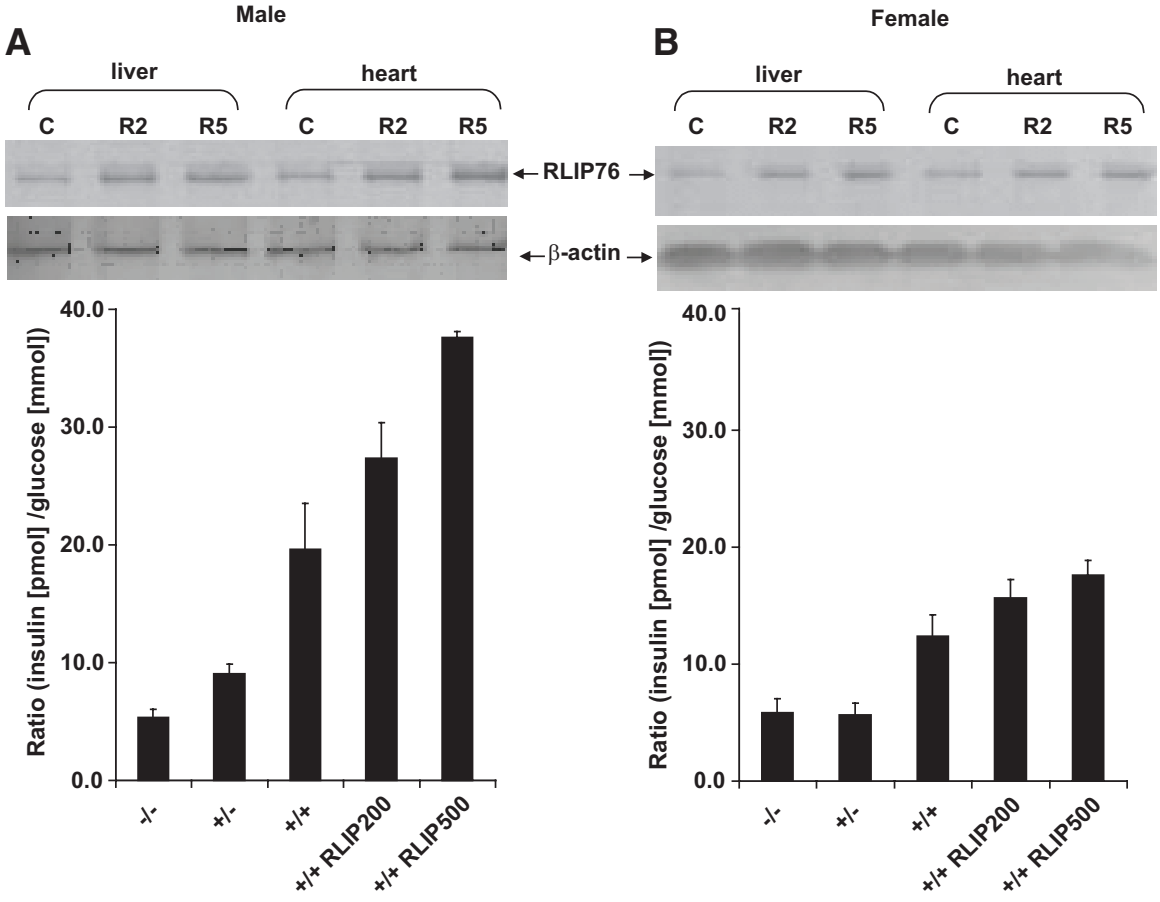

FIG. 3. Insulin-to-glucose ratio in RLIP76-deficient and -supplemented mice. Twelve-week-old C57BL/6 mice born of heterozygous × heterozygous mating were genotyped by PCR. Insulin and glucose measurement in blood serum was performed on wild-type (RLIP76$^{+/+}$) animals killed 24 h after a single intraperitoneal injection of control or RLIP76 liposomes equivalent to 200 and 500 μg RLIP76 protein. Insulin and glucose measurement in blood serum was also performed on heterozygous (RLIP76$^{+/-}$) and homozygous (RLIP76$^{-/-}$) animals. The values are presented as means ± SD from three separate determinations with three replicates (n = 9) (*A* and *B*). Western blot analyses for RLIP76 were performed on liver and heart tissues of RLIP76$^{+/+}$ male and female mice killed 24 h after administration of 200 or 500 μg RLIP76 protein in the form of liposomes, intraperitoneally. Aliquots of 100 μg detergent-solubilized crude membrane fraction from the liver and heart of animals treated with 200 μg (R2) or 500 μg (R5) were loaded per lane in SDS-PAGE, transblotted, and probed using anti-RLIP76 IgG primary and peroxidase-conjugated goat anti-rabbit IgG secondary antibody. The blots were developed with 4-chloro-1-napthol as chromogenic substrate (*A* and *B insets*). β-actin expression was used as loading control. Statistical analyses by ANOVA were significant at $P < 0.01$ for RLIP76$^{-/-}$ vs. RLIP76$^{+/-}$, RLIP76$^{-/-}$ vs. RLIP76$^{+/+}$, RLIP76$^{+/-}$ vs. RLIP76$^{+/+}$, and RLIP76$^{+/+}$ vs. RLIP76 proteoliposome–treated RLIP76$^{+/+}$.

2. However, the insulin sensitivity was magnified in RLIP76$^{-/-}$ mice, all of whom died of profound hypoglycemia within 90 min of insulin injection on the second day (Fig. 1*C*). These remarkable results indicated that RLIP76$^{-/-}$ mice are more insulin sensitive, and suggested that RLIP76 could function to antagonize insulin.

RLIP76 gene interruption improves glucose tolerance and plasma lipid levels. Additional evidence for insulin sensitivity was sought in studies of glucose tolerance. Blood glucose levels after oral challenge of 2 g/kg body wt glucose were consistently and significantly lower in the RLIP76$^{-/-}$ compared with wild type (Fig. 2*A*) ($P <$ 0.001). In the nonfasting state, blood glucose in RLIP76$^{-/-}$ mice was 46% lower in this study (Fig. 2*B*), consistent with the results above (Fig. 1). Fasting blood glucose in the RLIP76$^{-/-}$ mice decreased by <10%, whereas RLIP76$^{+/+}$ mice had a 35% reduction upon fasting. In addition, RLIP76$^{-/-}$ mice had lower total serum cholesterol and triglycerides (43 and 40% of control, respectively; $P <$ 0.01) (Fig. 2*C* and *D*). The hypoglycemia is particularly remarkable because oxidative stress (levels of lipid hydroperoxides, lipid alkenals, and alkenal-glutathione conjugates) is remarkably increased in the tissues of RLIP76$^{-/-}$ animals (23,27,33,34). This observation implies that in the absence of RLIP76, increases in these lipid-peroxidation products are insufficient by themselves to turn on any signaling pathway that can increase blood glucose or lipids.

RLIP76 protein level correlates with insulin-glucose ratio. The ratio of insulin to blood glucose (a measure of insulin resistance) was lower in RLIP76$^{+/-}$ or RLIP76$^{-/-}$ mice compared with RLIP76$^{+/+}$ animals ($P < 0.001$) (Fig. 3*A*). Insulin levels in all females were lower and less affected by the loss of RLIP76 (Fig. 3*B*). Insulin sensitivity appeared to increase with loss of RLIP76. Thus, we predicted that increasing tissue RLIP76 should increase insulin resistance. We examined the effect of augmenting RLIP76 in RLIP76$^{+/+}$ animals using intraperitoneal injection of purified recombinant human RLIP76 protein encapsulated in liposomes (Fig. 3). Previous studies have defined the purity, stability, and tissue pharmacology for RLIP76 delivery by these liposomes (22,27,35,36). Blood glucose measurements were performed 24 h after intraperitoneal injection of liposomes prepared with or without RLIP76 protein. Western blots of tissue homogenates and specific enzyme-linked immunosorbent assays showed sig-

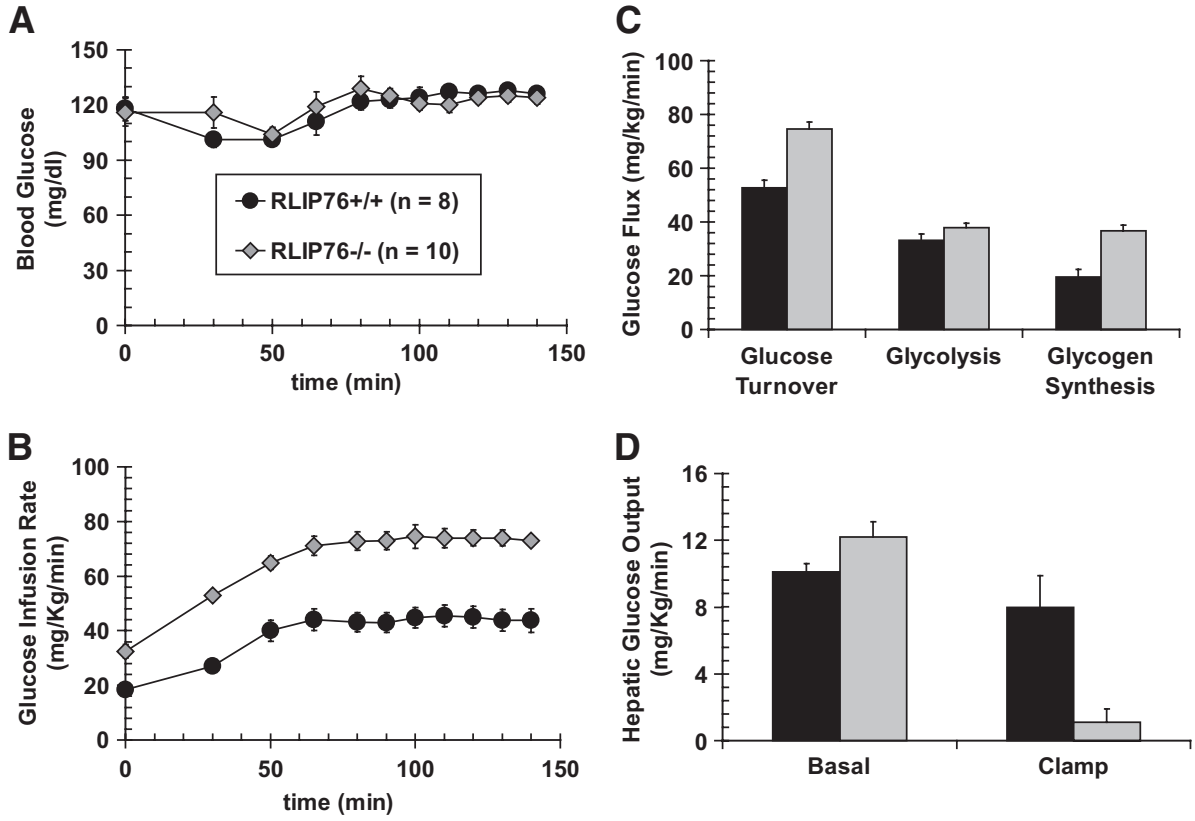

FIG. 4. Hyperinsulinemic-euglycemic and hyperglycemic clamp studies. Glucose and insulin clamp studies were performed as described in the RESEARCH DESIGN AND METHODS section at the Mouse Metabolic Phenotyping Center at the Yale University School of Medicine, with procedures approved by Yale University Institutional Animal Care and Use Committee. Panels *A* and *B* demonstrate the result of the hyperinsulinemic-euglycemic clamp study in which blood glucose of both wild-type (○) and RLIP76$^{-/-}$ (◇) animals was maintained at approximately equal levels for the 140-min duration of the study (*A*); the rate of glucose infusion required to maintain equal blood glucose (*B*) was significantly greater for the RLIP76$^{-/-}$ animals compared with wild-type controls at all experimental time points. Calculated total body glucose turnover, glycolysis, and hepatic glycogen synthesis (*C*), and hepatic glucose output in a basal (fasting) as well as hyperglycemic clamp (fed) state (*D*) are presented. RLIP76$^{+/+}$ mice, ■; RLIP76$^{-/-}$ mice, ▨. Statistical analyses by ANOVA were significant at $P < 0.05$ for RLIP76$^{+/+}$ vs. RLIP76$^{-/-}$; $n = 8$.

nificantly augmented RLIP76 in mouse tissues at 24 h after intraperitoneal injection (Fig. 3*A* and *B*, insets). The insulin/glucose ratio was increased in a stepwise fashion with respect to RLIP76 dose, also more prominently in males than females. Greater insulin sensitivity of knockout mice was confirmed by quantitative insulin sensitivity check index (QUICKI) (37) as well as homeostasis model assessment (HOMA) (38) analyses for insulin resistance as well. These findings indicated that increased tissue RLIP76 increases insulin resistance.

Hyperinsulinemic-euglycemic and hyperglycemic clamp studies demonstrate peripheral and hepatic insulin sensitivity of RLIP76$^{-/-}$ mice. Glucose homeostasis was compared in RLIP76$^{+/+}$ versus RLIP76$^{-/-}$ mice using hyperinsulinemic-euglycemic and hyperglycemic clamp. The RLIP76$^{-/-}$ mice were smaller and had lower fat and muscle mass. Glucose clamp was successful in maintaining stable blood glucose during the 140-min study (Fig. 4*A*). The glucose infusion rate required to maintain the same glucose level was almost twofold greater in the RLIP76$^{-/-}$ mice (Fig. 4*B*). The whole-body insulin sensitivity index, total peripheral-glucose uptake, hepatic glycolysis, glycogen synthesis, and hepatic insulin sensitivity index in the basal state were also greater in RLIP76$^{-/-}$ mice (Fig. 4*C*). Under glucose clamp conditions, hepatic glucose output was markedly reduced in RLIP76$^{-/-}$ animals (Fig. 4*D*). The remarkable difference indicates that RLIP76 functions to inhibit the turning off of gluconeogenesis during the fed state. Because RLIP76 is a stress-inducible protein, these findings strongly indicate that conditions of stress that may increase hepatic RLIP76 levels would tend to antagonize the normal decrease in hepatic gluconeogenesis in the fed state, potentially exacerbating stress hyperglycemia.

Cortisol-induced hyperglycemic response is intact in RLIP76$^{-/-}$ animals. The above observations led to the obvious question of how RLIP76 interacts with cortisol, the most important stress-protective hormone, as well as the hepatic enzymes that regulate gluconeogenesis, PEPCK, G6Pase, and F-1,6-BPase. Cortisol-induced hyperglycemia was preserved in RLIP76$^{-/-}$ animals, which had a similar degree of cortisol-induced rise in blood glucose as RLIP76$^{+/+}$ (Fig. 5).

RLIP76$^{-/-}$ mice have lower activity of PEPCK, F-1,6-BPase, and G6Pase. Although RLIP76 and cortisol effects on blood glucose appeared independent, it was clear that the absolute blood glucose in cortisol-treated RLIP76$^{+/+}$ animals was greater than could be achieved in RLIP76$^{-/-}$ animals. We reasoned that this could be due to effects of RLIP76 loss on the three principal enzymes that regulate hepatic gluconeogenesis, PEPCK, F-1,6-BPase, and G6Pase. To address this possibility, we compared the mRNA levels and activity of these enzymes between RLIP76$^{+/+}$ and RLIP76$^{-/-}$ mouse liver tissue. There was no difference in expression of PEPCK, F-1,6-BPase, or G6Pase mRNA (Fig. 6*A*); despite this, the specific activity

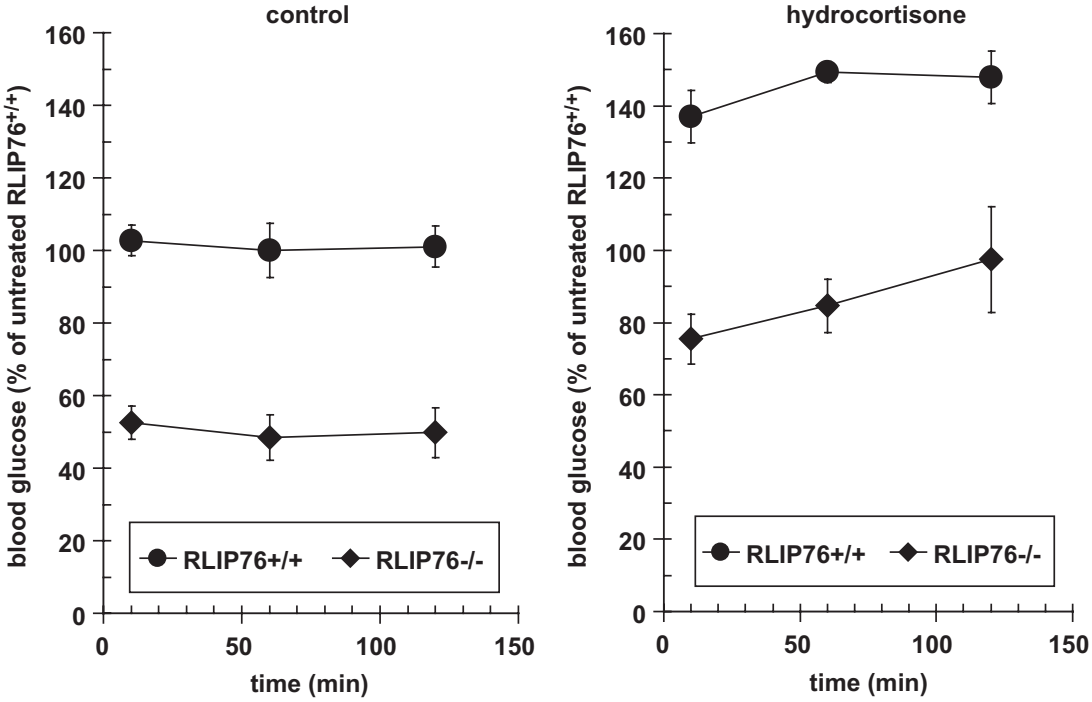

FIG. 5. The effect of hydrocortisone on the blood glucose level of RLIP76$^{+/+}$ and RLIP76$^{-/-}$ animals. Wild-type and RLIP76 knockout mice were treated with hydrocortisone (1 g/kg body wt) and the blood glucose level was checked in the blood drawn from the tail at different time points from 0 to 120 min. $P < 0.01$, compared RLIP76$^{+/+}$ vs. RLIP76$^{-/-}$ animals; $n = 5$.

of all three proteins was substantially lower in the RLIP76$^{-/-}$ mouse liver. Comparison of these activities in RLIP76$^{+/+}$ versus RLIP76$^{-/-}$ mouse liver homogenate treated without or with overnight dialysis showed that dialyzable inhibitors were present but could not account for the lower activity of these enzymes in RLIP76$^{-/-}$. 4-HNE, an alkenal shown to increase twofold to threefold in RLIP76$^{-/-}$ mouse liver (33,34), did not directly affect the activity of PEPCK or G6Pase but activated F-1,6-BPase activity. It is remarkable that despite decreased activity of these key gluconeogenic enzymes, hepatic glucose output was clearly increased in the knockout animals (Fig. 6*B*–*E*).

Baseline and oxidative stress–induced insulin endocytosis is deficient in RLIP76$^{-/-}$ MEFs. Our previous studies in MEFs derived from RLIP76$^{-/-}$ and RLIP76$^{+/+}$ mice have shown that clathrin-dependent endocytosis of epidermal growth factor receptor is markedly decreased in RLIP76$^{-/-}$ MEFs. Because clathrin-dependent endocytosis has been shown to be a primary mechanism for uptake of the insulin/insulin-receptor complex (thus terminating, or antagonizing, insulin signaling), we compared the uptake of fluorescein-labeled insulin between RLIP76$^{+/+}$ and RLIP76$^{-/-}$ MEFs. Results of these studies confirmed that insulin endocytosis is clearly deficient in RLIP76$^{-/-}$ MEFs (Fig. 7*A*). Oxidative stress in the form of hydrogen peroxide exposure caused a marked increase in endocytosis of quantum dot–labeled insulin-rhodamine in the RLIP76$^{+/+}$ MEFs, whereas this stress-mediated effect was absent in RLIP76$^{-/-}$ MEFs (Fig. 7*B*). Taken together, these results offer strong support for a model in which RLIP76 functions to antagonize insulin signaling, and that stress conditions known to induce RLIP76 would tend to exacerbate insulin resistance (20,26,39).

Analysis of interactions among RLIP76, its transported substrates, and insulin by FRET. To directly determine whether RLIP76 migrated with insulin in the endocytic vesicle, we expressed GFP-RLIP76 into RLIP76$^{-/-}$ MEFs and examined the endocytosis of rhodamine-labeled insulin using confocal laser microscopy and FRET analysis (Fig. 7*C*). These studies also demonstrated that the internalization of rhodamine-labeled insulin was also deficient in RLIP76$^{-/-}$ MEFs. Whereas empty green fluorescent protein (GFP) vector protein did not affect the internalization of rhodamine-insulin, transfection of RLIP76-GFP restored the internalization of insulin.

Because insulin is present on the outside of the cell membrane and RLIP76 is associated with the endocytosis machinery on the inner membrane leaflet, we predicted that although the red and green fluorescence is internalized together, there should be no direct FRET interaction between the red and green because the distance between the two fluorescent ligands should exceed 100 nm. Results of FRET analysis were consistent with this prediction (Fig. 7*D*).

FRET analysis can demonstrate specific binding of transported substrates to RLIP76. The validity of the FRET analysis was confirmed using the fluorescent anthracycline drug, DOX, which is known to bind to RLIP76 as well as GSH-monochlorobimane. Results of FRET studies are presented in Fig. 8. The top images show the observed intensities for respective samples, and below the histogram graph presents observed fluorescence lifetime measured for the respective images (Fig. 8*A* and *B*). For monochlorobimane (MCB) alone (histogram in red), the signal is very bright and the fluorescence lifetime is long, as expected, ~9 ns with relatively narrow distribution (Fig. 8*B*). Addition of RLIP76-GFP results in dramatic shortening of MCB fluorescence lifetime, which drops to ~4 ns (histogram in red). The lifetime distribution is now relatively broad. This could reflect small heterogeneity of distances and/or relative orientations between MCB chro-

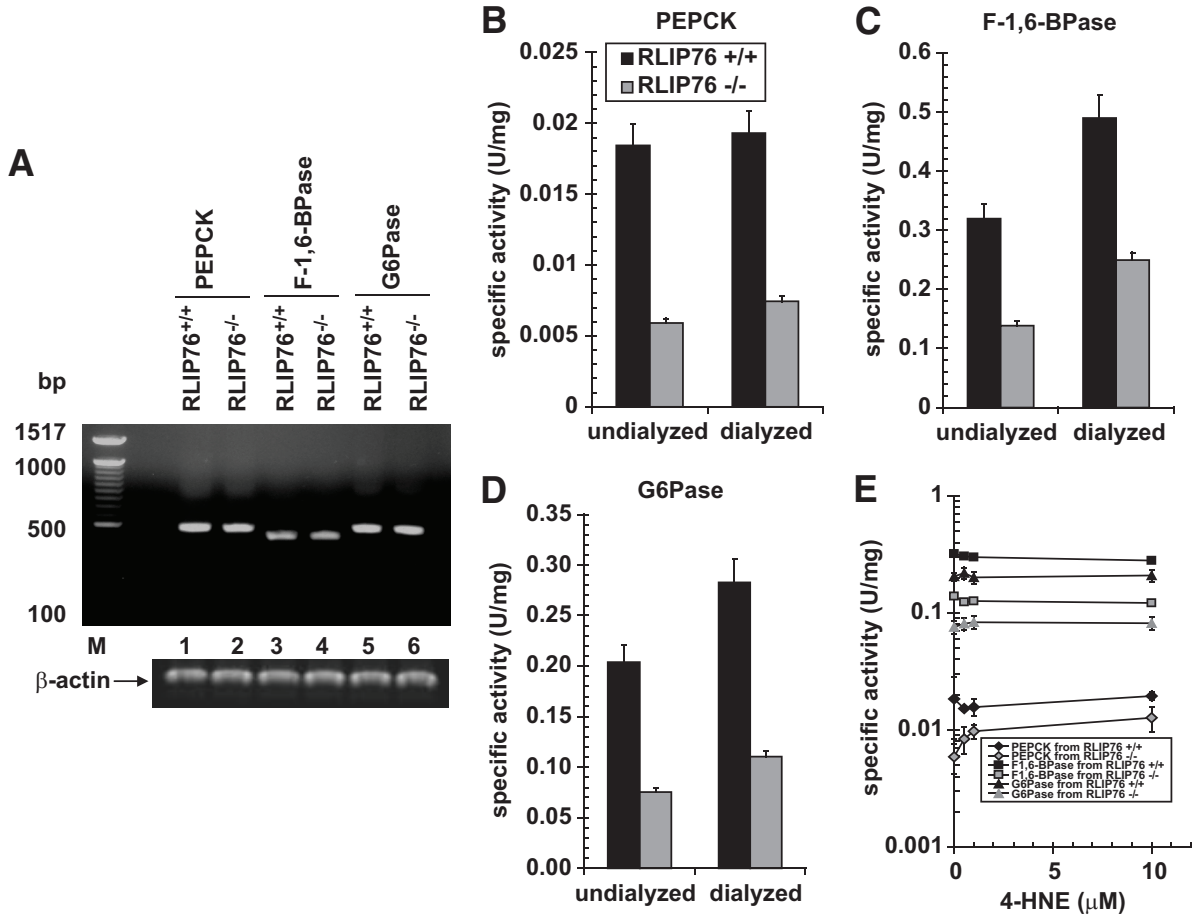

FIG. 6. The activity of gluconeogenesis enzymes. The activity of PEPCK (*B*), F-1,6-BPase (*C*), and G6Pase (*D*) was measured in undialyzed and dialyzed liver homogenates of RLIP76$^{+/+}$ and RLIP76$^{-/-}$ animals. The effect of 4-HNE was also determined on the activity for all three important enzymes of gluconeogenesis (*E*). The enzyme PEPCK catalyzes the conversion of phosphoenolpyruvate to fructose1,6-biphosphate in a series of steps involving oxidation of NADH to NAD. In this assay, the loss of NADH was determined spectrophotometrically by measuring absorbance at 340 nm, based on the method of Opie and Newsholme (29). For F-1,6-BPase activity, a spectrophotometric-coupled enzyme assay was used based on the method of Taketa and Pogell (30). F-1,6-BPase activity was coupled with phosphoglucose isomerase and NADP-dependent glucose 6-phosphate dehydrogenase, and NADPH formation was measured at 340 nm. G6Pase activity was determined spectrophotometrically using the method of Gierow and Jergil (31). The method is based on a coupled enzyme reaction in which glucose formed is reacted with glucose oxidase and peroxidase, and the quinoneimine formed is a colored product and its formation can be followed spectrophotometrically at 510 nm. The expression of all three enzymes was determined by RT-PCR using their gene-specific primers (*A*). Either dialyzed or undialyzed, $P < 0.01$, when compared with RLIP76$^{+/+}$ vs. RLIP76$^{-/-}$. RLIP76$^{+/+}$ or RLIP76$^{-/-}$, $P < 0.07$, when compared with undialyzed vs. dialyzed. Means ± SD for three separate experiments, each in triplicate, are shown; $n = 9$.

mophore and GFP. Such shortening of donor fluorescence lifetime indicates strong interaction (very close proximity of two molecules), which is entirely consistent with our hypothesis. The right lower panel (Fig. 8*C*) shows the lifetime histogram for GFP only (green) and fluorescence of GFP in the presence of DOX (blue). The fluorescence lifetime of GFP in the presence of DOX is shorter, confirming that DOX clearly did interact with the green fluorescence protein of RLIP76. The interaction of GSH-monochlorobimane fluorescent conjugate was much more clearly evident and indicated specific binding of the conjugate (Fig. 8*B*).

Effect of RLIP76 loss or augmentation on basal and insulin-stimulated change in glucose uptake and RTK signaling. RLIP76$^{+/+}$ and RLIP76$^{-/-}$ MEFs were transfected with pcDNA3.1 empty vector (V) or pcDNA3.1 with full-length RLIP76 cDNA (R) using Lipofectamine (Invitrogen). Western blot analyses of the 28,000*g* crude supernatant of homogenate of these cells against anti-RLIP76 IgG demonstrated the absence of RLIP76 antigen in RLIP76$^{-/-}$ MEFs, and showed increased RLIP76 protein upon transfection in both RLIP76$^{+/+}$ an RLIP76$^{-/-}$ MEFs (Fig. 9*A*). A factorial experiment (2 [genotype] × 2 [RLIP76 overexpression] × 2 [anti-RLIP76 antibody] × 2 [insulin]) was designed to measure and compare the effect of insulin on glucose uptake, Foxo-1 inactivation, and activation of Akt, Jun NH_2-terminal kinase (JNK, and Hsf-1. The results, normalized to the control group, RLIP76$^{+/+}$ MEFs transfected with empty vector, treated with no insulin and preimmune IgG are presented (Fig. 9*B*–*D*). In control RLIP76$^{+/+}$ MEFs, treatment with anti-RLIP76 IgG, previously shown to inhibit the transport activity of RLIP76 by binding to a cell surface epitope, caused a significant increase in activation of Hsf-1, JNK, and Akt, a slight suppression of Foxo, and a 40% increase in uptake of glucose, in the absence of insulin. This finding indicated that inhibition of RLIP76 in normal cells activates stress pathways, and increases uptake of glucose through an insulin-independent mechanism. Insulin caused the expected effects of a more than twofold increase in glucose uptake, accompanied by activation of Hsf-1, Akt, and JNK, and inactivation of Foxo. In the presence of both insulin and anti-RLIP76 IgG, glucose uptake as well as signaling

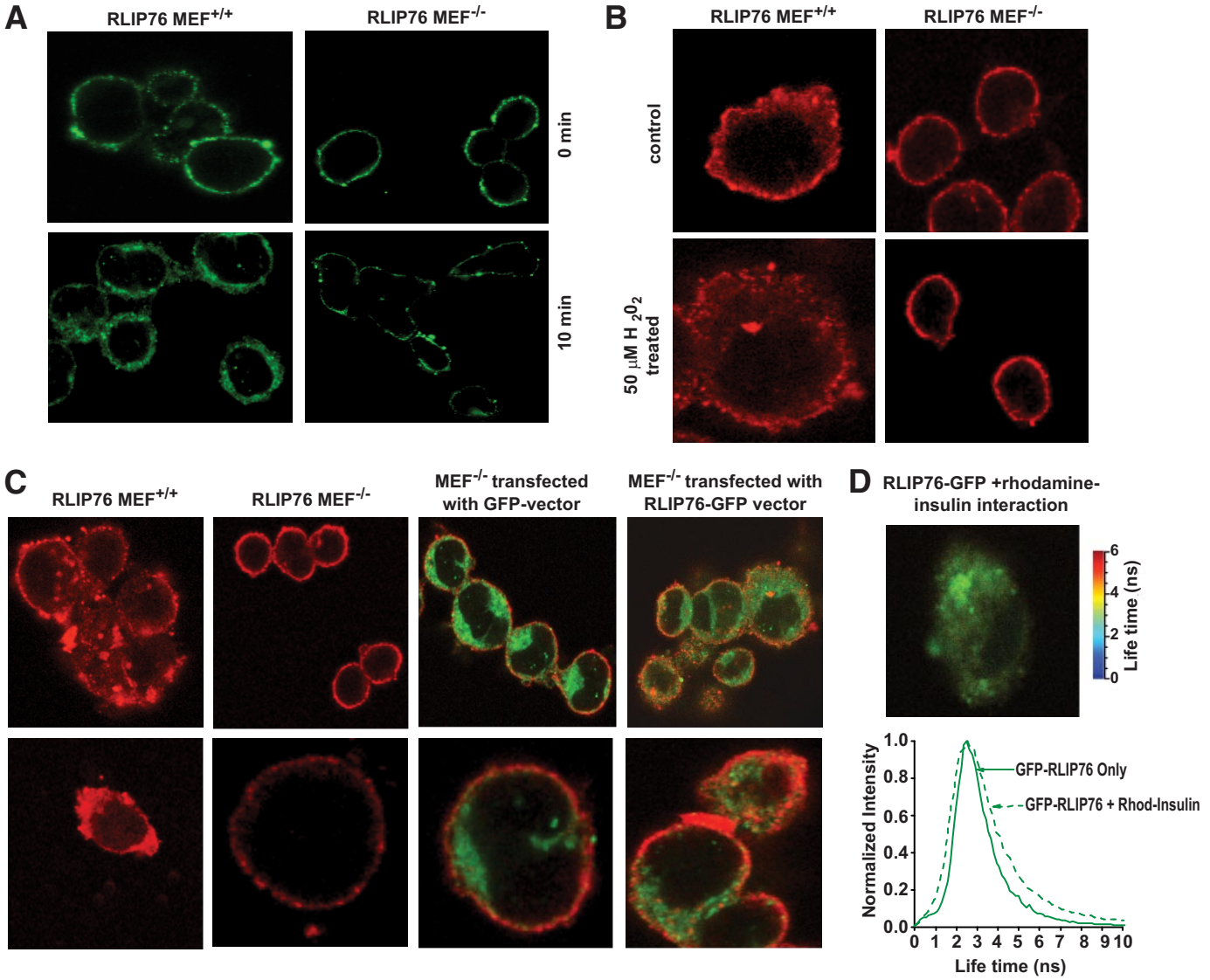

FIG. 7. Effect of RLIP76 on insulin internalization. Insulin binding and internalization were studied in RLIP76 MEF$^{+/+}$ and RLIP76 MEF$^{-/-}$ using FITC-insulin. Cells (0.1 × 10^6 cells/ml) grown on the sterilized coverslips were incubated with FITC-insulin (100 ng/ml) for 45 min in ice followed by incubation for 10 min at 37°C. Cells were fixed and analyzed by confocal laser microscopy. Photographs taken at identical exposure at ×400 magnification are presented (*A*). Stress-mediated effect on insulin internalization. RLIP76$^{+/+}$ and RLIP76$^{-/-}$ MEFs (0.1 × 10^6 cells/ml) were grown on coverslips, followed by incubation with 50 μmol/l H_2O_2 for 20 min at 37°C, and were allowed to recover for 2 h. Cells were treated with molar ratio 6:1 of insulin-rhodamine:QD on ice for 45 min, washed, incubated for 10 min at 37°C, and fixed in cold 4% paraformaldehyde. Slides were analyzed using confocal laser-scanning microscopy. Photographs taken at identical exposure at ×400 magnification are presented (*B*). Effect of RLIP76 on insulin internalization using insulin-QD complexes. Insulin binding and internalization were studied in MEF$^{+/+}$, MEF$^{-/-}$, and MEF$^{-/-}$ transfected with empty GFP vector and RLIP76-GFP vector, using insulin-QD complexes. Insulin-QD complexes were formed by incubation of insulin (40 nmol/l; Life Technologies) with QDs 605 ITK amino (PEG; Molecular Probes) at 4°C for 30 min. A molar ratio of 6:1 of insulin:QDs was used. Cells grown on the sterilized coverslips were treated with insulin-QD complexes for 10 min at 37°C. Cells were fixed and analyzed using confocal laser scanning microscopy with Zeiss 510 meta system, with excitation at 594 nm and emission at 610 nm. Photographs taken at identical exposure at ×400 magnification are presented (*C*). The molecular interactions between the RLIP76 and insulin were checked by FRET analysis as described in the RESEARCH DESIGN AND METHODS section. The FRET analysis clearly indicated that there is no direct interaction of RLIP76 and insulin (*D*). (A high-quality digital representation of this figure is available in the online issue.)

changes were greater than with either agent alone, and the net effect was consistent with an additive effect.

RLIP76 overexpression in the RLIP76$^{+/+}$ MEFs caused an effect opposite to that of the antibody, a suppression of Hsf-1, JNK, and Akt, and activation of Foxo, as well as a reduction of glucose uptake to half that seen with empty vector transfection. Treatment of RLIP76-overexpressing RLIP76$^{+/+}$ MEFs with antibody restored Hsf-1, Akt, and JNK as well as glucose uptake to slightly greater than control. Treatment with insulin resulted in expected increase in Hsf-1, Akt, and JNK and decrease in Foxo, but the magnitude of this response was suppressed significantly. Most strikingly, the glucose uptake in response to insulin, although ~1.8-fold compared with the absence of insulin, was still less than the control, and only one-third of that seen in empty vector–transfected cells. As in the vector-transfected cells, anti-RLIP76 IgG pretreatment resulted in augmentation of insulin response with respect to Hsf-1, JNK, and Akt, but suppression of Foxo was less prominent compared with control. These observations argue strongly for the assertion that RLIP76 functions to antagonize insulin signaling broadly and directly, and that conditions in which RLIP76 is elevated result in decreased response to insulin (resistance). Furthermore, RLIP76 also

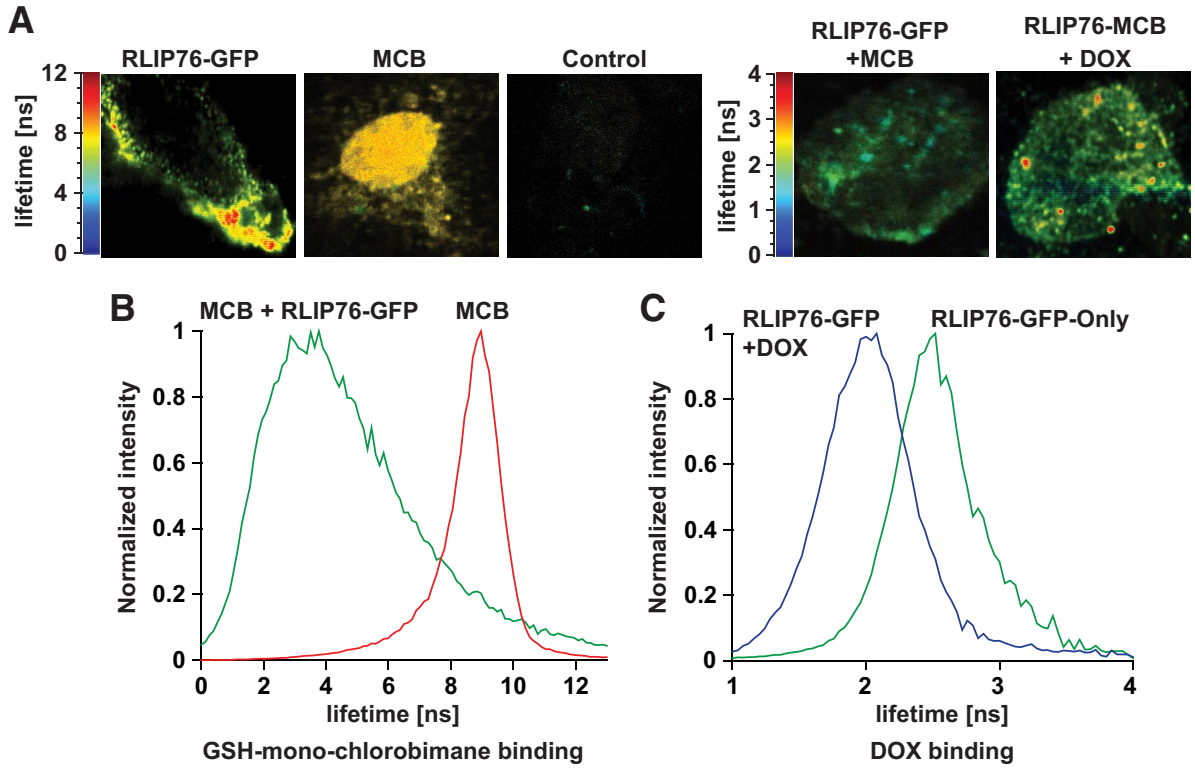

FIG. 8. Binding of GSH-monochlorobimane and DOX by FRET analysis. Binding of GSH-monochlorobimane (GSH-MCB) and DOX was studied in MEF$^{-/-}$ and MEF$^{-/-}$ transfected with RLIP76-GFP vector. Cells grown on the sterilized coverslips were treated with either 50 μmol/l monochlorobimane or 10 μmol/l DOX and incubated at 37°C for 20 min. Cells were fixed with 4% paraformaldehyde, and FRET and molecular interactions in the cell were analyzed using time-resolved confocal microscope MT 200 (Picoquant) with pulsed diode laser excitations at 405 nm (for MCB donor) and 475 nm (for GFP donor). For MCB observation, 465-nm (10-nm bandwidth) interference filter crossed with 430-nm long path cutoff was used and for GFP observation, 490- to 530-nm interference filter crossed with 500-nm long path filter was used. The top images show the observed intensities for respective samples (*A*). Below the histogram, the graph presents observed fluorescence lifetime measured for the respective images. For MCB alone (histogram in red), the signal is very bright and fluorescence lifetime is long, as expected, ~9 ns with the relatively narrow distribution. Addition of RLIP76-GFP results in dramatic shortening of MCB fluorescence lifetime, which dropped to ~4 ns (histogram in red) (*B*). The validity of the FRET analysis was confirmed using the fluorescent anthracycline drug, DOX, which is known to bind to RLIP76. *C*: Lifetime histogram for GFP only (green) and fluorescence of GFP in the presence of DOX (blue). The fluorescence lifetime of GFP in the presence of DOX is shorter, confirming that DOX clearly did interact with the green fluorescence protein of RLIP76. (A high-quality digital representation of this figure is available in the online issue.)

functions to antagonize insulin-independent glucose uptake as might be expected if glucose transporters were also subjected to increased rate of endocytosis.

Consistent with this model, the comparison of RLIP76$^{+/+}$ MEFs with RLIP76$^{-/-}$ MEFs showed a higher baseline activation of Hsf-1, JNK, and Akt, and lower Foxo. Glucose uptake in the absence of insulin in the RLIP76$^{-/-}$ MEFs was 60% higher as well, indicating that the lack of RLIP76 results in a state in which basal (insulin-independent) uptake of glucose is increased. This is likely to be the major underlying explanation for fasting hypoglycemia and increased glucose utilization in RLIP76$^{-/-}$ mice. As expected, anti-RLIP76 IgG treatment of RLIP76$^{-/-}$ MEFs did not cause a significant change in the parameters measured. Insulin responsiveness with respect to changes in Hsf-1, JNK, Akt, and Foxo was preserved in RLIP76$^{-/-}$ cells, although the fold change in glucose uptake was actually slightly lower. This was due to a higher baseline insulin-independent signaling effects and glucose uptake, and a likely ceiling effect of maximal possible glucose uptake, possibly determined by the number of glucose transporters present for translocation to the membrane. The anti-RLIP76 IgG had no effect on these parameters in RLIP76$^{-/-}$ MEFs, indicating that observed effects of this antibody in RLIP76$^{+/+}$ MEFs are due to a specific interaction of these antibodies with RLIP76 rather than any nonspecific effect.

Transfection of RLIP76 into RLIP76$^{-/-}$ MEFs resulted in restoration of the pattern of signaling and glucose uptake rate to that found in control RLIP76$^{+/+}$ MEFs; after transfection with RLIP76, response to anti-RLIP76 IgG (in terms of increased glucose uptake and increased signaling) was restored. Although the magnitude of insulin response was blunted somewhat compared with the untransfected RLIP76$^{-/-}$ MEFs, transfection with RLIP76 caused a heightened response when cells were treated with both insulin and anti-RLIP76 IgG.

Taken together, these findings are consistent with a model in which RLIP76 functions to antagonize peripheral cellular glucose uptake through both insulin-dependent as well as insulin-independent mechanisms, and conditions that increased RLIP76 should result in reduced uptake of glucose in peripheral cells.

DISCUSSION

Our studies show that RLIP76 regulates blood glucose by controlling insulin-dependent and insulin-independent mechanisms of cellular glucose uptake in both peripheral and hepatic tissues. The striking lack of endocytosis in RLIP76$^{-/-}$ MEFs appears to be the major overall perturbation responsible for the observed global effects on glucose homeostasis and signaling. The central role of RLIP76 in glycemic regulation is also evident from para-

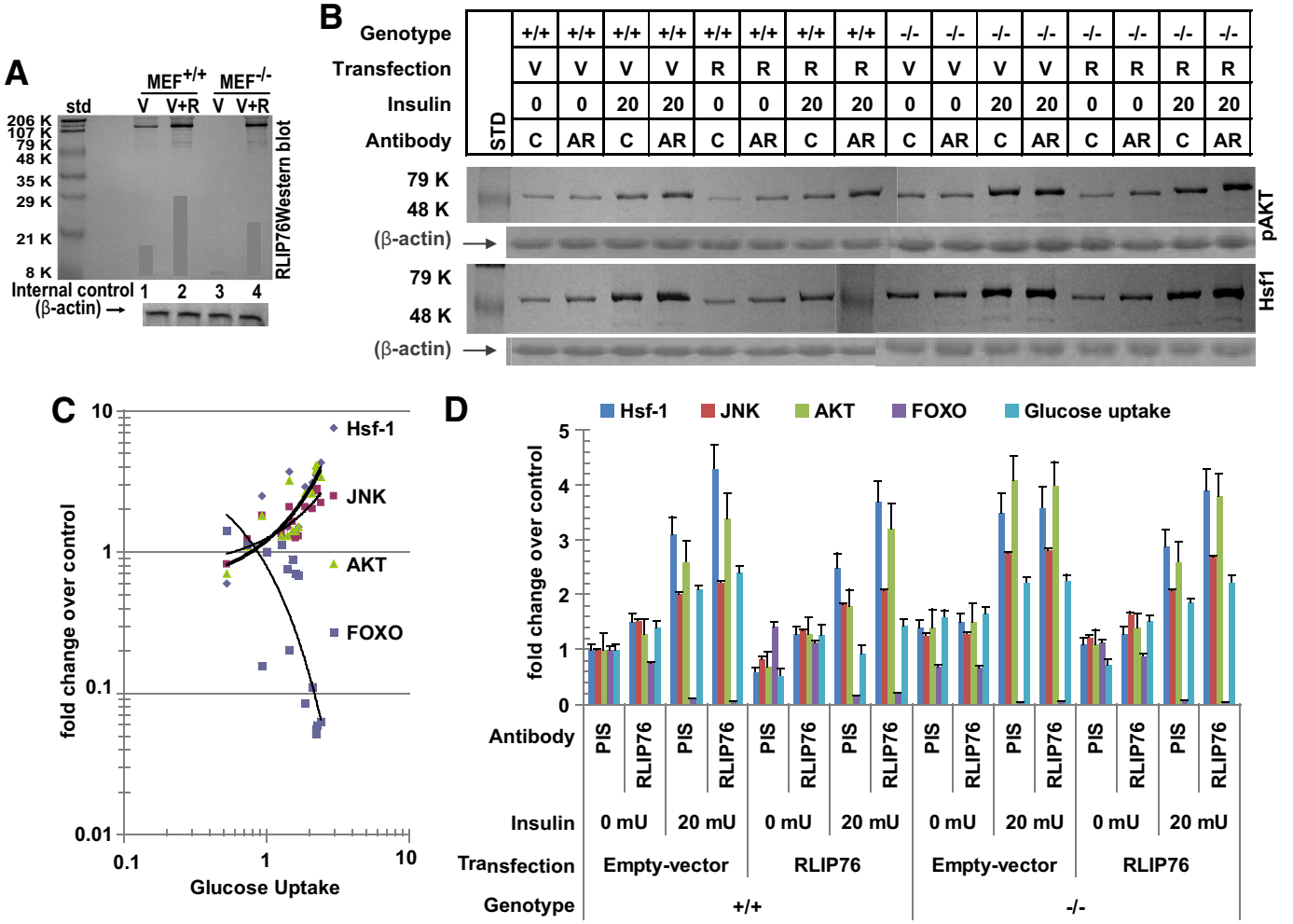

FIG. 9. Regulation of signaling via Hsf-1, Akt, JNK, and FOXO-1 by RLIP76. RLIP76$^{+/+}$ and RLIP76$^{-/-}$ MEFs were subjected to transfection with pcDNA3.1 empty vector (V) or pcDNA3.1 with full-length RLIP76 cDNA (R) using Lipofectamine (Invitrogen). Crude supernatant of 28,000*g* of these cells was subjected to Western blot analysis against anti-RLIP76 IgG to demonstrate the absence of RLIP76 antigen in RLIP76$^{-/-}$ MEFs and to show increased RLIP76 protein upon transfection in both RLIP76$^{+/+}$ and RLIP76$^{-/-}$ MEFs. β-Actin was used as an internal control (*A*). The effect of RLIP76 overexpression, insulin, or anti-RLIP76 antibody on RLIP76$^{+/+}$ and RLIP76$^{-/-}$ MEFs on signaling as well as glucose uptake was carried out at 37°C with 5% CO_2 atmosphere. The cells were pretreated with either polyclonal rabbit preimmune IgG (C or PIS) or anti-human RLIP76 IgG fractions (AR) (40 μg/ml final concentration) for 1 h. Buffer containing ^{14}C-glucose and either no insulin or 20 mU insulin was added to start the measurement of glucose uptake, and the measurement was terminated at 30 min by washing off the medium with ice-cold PBS and solubilization of cells in counting cocktail. Glucose uptake was measured in 5 × 10^6 cells, as described previously (36). In parallel experiments in which ^{14}C glucose was omitted, measurements of phosphorylation of Akt, Hsf-1, and JNK, and inactivation of Foxo1, were performed at 30 min. Results of Western blot analyses of Hsf-1 expression and phospho-Akt (Ser473; Millipore, Billerica, MA) are presented. β-actin expression was shown to confirm equal amount of protein was loaded in each sample (*B*). Results from all groups were analyzed with plots of glucose uptake vs. Hsf-1 expression and Akt activation as well as Foxo-1 inactivation and JNK phosphorylation (measured by ELISA; Active Motif, Carlsbad, CA) (*C*). Results of all five measurements normalized to the control group (RLIP76$^{+/+}$ MEFs transfected with empty vector, treated with no insulin and preimmune IgG) are presented (*D*). Means ± SD for two separate experiments, each in triplicate, are shown; *n* = 6 (33,36).

doxical findings, of marked insulin sensitivity despite the presence of several fold increased levels of oxidative stress–derived free radicals, lipid peroxidation products, and activated JNK, and p38 (23–27,33,39). If small-molecule products of oxidative degradation could themselves increase insulin resistance, we should expect that RLIP76$^{-/-}$ mice should be quite insulin resistant because they have several fold higher levels of tissue hydroperoxides compared with RLIP76$^{+/+}$ mice (23,33,34); this was obviously not the case.

To explain this apparent paradox, our model proposes that lipid peroxidation products mediate insulin resistance because their GS-E conjugates are necessary substrates for RLIP76 to drive the process of endocytosis—in the absence of RLIP76 and of endocytosis, the "dwell time" of insulin at the plasma membrane is greater, resulting in greater insulin sensitivity. Increasing RLIP76 in cells inhibits its insulin-independent glucose uptake, and antagonizes insulin-independent glucose uptake. Because clathrin-dependent endocytosis exerts broad effects on receptor-ligand signaling (including G-protein–linked receptors) as well as on trafficking of membrane proteins (such as GLUT), the insulin-independent effects are understandable, and in some ways expected. Because lipid trafficking between peripheral and hepatic tissues is also intricately linked with clathrin-dependent endocytosis (23–25,39), it is also perhaps not surprising that both blood cholesterol and triglycerides were lower in RLIP76$^{-/-}$ animals. These findings are of clinical interest because both hyperglycemia and hyperlipidemia could be treated by targeting RLIP76. Because RLIP76 is a known stress-inducible protein, conditions that increase RLIP76 expression (i.e., oxidative stress) will cause insulin resistance and hyperlipidemia. More importantly, in the absence of RLIP76,

oxidative stress alone is insufficient to mediate insulin resistance (23,26).

The central stress-response role of RLIP76 is also evident from the effects of RLIP76 loss on stress-responsive kinase signaling, which are activated but insufficient to mediate insulin resistance. Elevated heat shock proteins are expected because RLIP76 is known to bind to and sequester Hsf-1, the master transcriptional regulator of the heat shock response. Thus, RLIP76 functions as the primary regulator (inhibitor) of transcription of chaperones, which are dramatically increased in tissue of RLIP76$^{-/-}$ mice (33,36,39). Decreased levels of chaperone heat shock proteins have been correlated with insulin resistance (40); thus elevated chaperone levels could also contribute to the observed insulin sensitivity of RLIP76$^{-/-}$ mice. MEF studies show that Hsf-1, JNK, and Akt are activated, and their activation is directly correlated with glucose uptake in response to insulin; FOXO is inactivated by insulin, and its activity is inversely correlated with insulin-dependent glucose uptake. All signaling responses are blunted by RLIP76 overexpression, again emphasizing the overarching role of clathrin-dependent endocytosis in signaling regulation, and the crucial rate-regulatory role of RLIP76 in clathrin-dependent endocytosis.

Increased insulin sensitivity in short-term (clamp studies) in both peripheral and hepatic tissues of C57B mice, and the dramatic effects of repeat insulin administration in RLIP76$^{-/-}$ animals, are entirely consistent with our model. In the absence of RLIP76, in the fed state, hepatic glucose output is nearly abrogated in RLIP76$^{-/-}$ mice, whereas it is only slightly suppressed in RLIP76$^{+/+}$; these findings imply that inhibition of RLIP76 could have a salutary effect by reducing hepatic glucose output. The complex interactions of insulin-dependent and insulin-independent regulators of glycemic control in the whole animal are likely to yield interesting and perhaps paradoxical observations, with further experimental manipulations planned to evaluate the effects of RLIP76 loss on interactions among diet, insulin, glucagon, and glucocorticoids.

Glucocorticoid-mediated hyperglycemia is known to be mediated both through increased gluconeogenesis (41) and through increased insulin resistance (42). Diminished hyperglycemic effect of hydrocortisone in RLIP76$^{-/-}$ mice indicates a regulatory role of RLIP76 in glucocorticoid action. It should be noted that glucocorticoid receptor knockout mice are hypoglycemic only when stressed; RLIP76$^{-/-}$ mice are hypoglycemic at baseline—despite the fact that they have relatively higher hepatic glucose output than the RLIP76$^{+/+}$ mice. These observations imply a fundamental increase in both hepatic and peripheral insulin sensitivity in RLIP76$^{-/-}$ mice.

Present studies have important implications in the understanding of mechanisms governing the phenomenon of insulin resistance associated with clinical disease conditions in which oxidative stress is increased. They predict that an invariable consequence of oxidative stress is an increase in formation of GS-E conjugates in cells, resulting in an increased rate of their efflux, and a consequent increase in the rate of internalization of membrane receptor/ligand complexes; by the same token, conditions or agents that reduce oxidative stress and GS-E conjugate formation should result in an increased dwell time of receptor/ligand couples in plasma membrane, increasing signaling efficiency. Another important corollary to present findings is that small molecules that interact with RLIP76, either at the cell surface or internally at one or more sites known to regulate its transport activity, could potentially function as novel hypoglycemic and hypolipidemic agents.

ACKNOWLEDGMENTS

This work was supported in part by grants from the National Institutes of Health CA-77495 and CA-104661 (to S.A.) and ES-012171 (to Y.C.A.), the Cancer Research Foundation of North Texas (to S.S.S. and S.Y.), the Institute for Cancer Research, and the Joe & Jessie Crump Fund for Medical Education (to S.S.S.).

No potential conflicts of interest relevant to this article were reported.

We thank the Center for Commercialization of Fluorescence Technologies at the University of North Texas Health Science Center, Fort Worth, Texas, for helping with confocal laser and FRET analyses. We also thank Abhijit Bugde and Dr. Kate Luby-Phelps from The Live Cell Imaging Core Facility at The University of Texas Southwestern Medical Center at Dallas for help in imaging using the Leica TCS SP5 confocal microscope.

REFERENCES

1. Tirosh A, Potashnik R, Bashan N, Rudich A. Oxidative stress disrupts insulin-induced cellular redistribution of insulin receptor substrate-1 and phosphatidylinositol 3-kinase in 3T3–L1 adipocytes: a putative cellular mechanism for impaired protein kinase B activation and GLUT4 translocation. J Biol Chem 1999;274:10595–10602
2. Awasthi S, Singhal SS, Srivastava SK, Zimniak P, Bajpai KK, Saxena M, Sharma R, Ziller SA 3rd, Frenkel EP, Singh SV. Adenosine triphosphate-dependent transport of doxorubicin, daunomycin, and vinblastine in human tissues by a mechanism distinct from the P-glycoprotein. J Clin Invest 1994;93:958–965
3. Yung LM, Leung FP, Yao X, Chen ZY, Huang Y. Reactive oxygen species in vascular wall. Cardiovasc Hematol Disord Drug Targets 2006;6:1–19
4. Seddon M, Looi YH, Shah AM. Oxidative stress and redox signalling in cardiac hypertrophy and heart failure. Heart 2007;93:903–907
5. Ceriello A. Acute hyperglycaemia and oxidative stress generation. Diabet Med 1997;14(Suppl. 3):S45–S49
6. Tirosh A, Rudich A, Potashnik R, Bashan N. Oxidative stress impairs insulin but not platelet-derived growth factor signalling in 3T3–L1 adipocytes. Biochem J 2001;355:757–763
7. Evans JL, Goldfine ID, Maddux BA, Grodsky GM. Are oxidative stress-activated signaling pathways mediators of insulin resistance and beta-cell dysfunction? Diabetes 2003;52:1–8
8. Talior I, Yarkoni M, Bashan N, Eldar-Finkelman H. Increased glucose uptake promotes oxidative stress and PKC-delta activation in adipocytes of obese, insulin-resistant mice. Am J Physiol Endocrinol Metab 2003;285: E295–E302
9. Tiedge M, Lortz S, Drinkgern J, Lenzen S. Relation between antioxidant enzyme gene expression and antioxidative defense status of insulin-producing cells. Diabetes 1997;46:1733–1742
10. Maechler P, Jornot L, Wollheim CB. Hydrogen peroxide alters mitochondrial activation and insulin secretion in pancreatic beta cells. J Biol Chem 1999;274:27905–27913
11. Sakai K, Matsumoto K, Nishikawa T, Suefuji M, Nakamaru K, Hirashima Y, Kawashima J, Shirotani T, Ichinose K, Brownlee M, Araki E. Mitochondrial reactive oxygen species reduce insulin secretion by pancreatic beta-cells. Biochem Biophys Res Commun 2003;300:216–222
12. Paz K, Hemi R, LeRoith D, Karasik A, Elhanany E, Kanety H, Zick Y. A molecular basis for insulin resistance: elevated serine/threonine phosphorylation of IRS-1and IRS-2 inhibits their binding to the juxtamembrane region of the insulin receptor and impairs their ability to undergo insulin-induced tyrosine phosphorylation. J Biol Chem 1997;272:29911–29918
13. Evans JL, Maddux BA, Goldfine ID. The molecular basis for oxidative stress-induced insulin resistance. Antioxid Redox Signal 2005;7:1040–1052
14. Pessler D, Rudich A, Bashan N. Oxidative stress impairs nuclear proteins binding to the insulin responsive element in the GLUT4 promoter. Diabetologia 2001;44:2156–2164
15. Frey RS, Gao X, Javaid K, Siddiqui SS, Rahman A, Malik AB. Phosphatidylinositol 3-kinase gamma signaling through protein kinase Czeta induces

NADPH oxidase-mediated oxidant generation and NF-kappaB activation in endothelial cells. J Biol Chem 2006;281:16128–16138
16. Liochev SI, Fridovich I. How does superoxide dismutase protect against tumor necrosis factor: a hypothesis informed by effect of superoxide on "free" iron. Free Radic Biol Med 1997;23:668–671
17. Esterbauer H, Schaur RJ, Zollner H. Chemistry and biochemistry of 4-hydroxynonenal, malonaldehyde and related aldehydes. Free Radic Biol Med 1991;11:81–128
18. Awasthi YC, Yang Y, Tiwari NK, Patrick B, Sharma A, Li J, Awasthi S. Regulation of 4-hydroxynonenal-mediated signaling by glutathione S-transferases. Free Radic Biol Med 2004;37:607–619
19. Feng Z, Hu W, Tang MS. Trans-4-hydroxy-2-nonenal inhibits nucleotide excision repair in human cells: a possible mechanism for lipid peroxidation-induced carcinogenesis. Proc Natl Acad Sci U S A 2004;101:8598–8602
20. Cheng JZ, Sharma R, Yang Y, Singhal SS, Sharma A, Saini MK, Singh SV, Zimniak P, Awasthi S, Awasthi YC. Accelerated metabolism and exclusion of 4-hydroxynonenal through induction of RLIP76 and hGST5.8 is an early adaptive response of cells to heat and oxidative stress. J Biol Chem 2001;276:41213–41223
21. Singhal SS, Sehrawat A, Mehta A, Sahu M, Awasthi S. Functional reconstitution of RLIP76 catalyzing ATP-dependent transport of glutathione-conjugates. Int J Oncol 2009;34:191–199
22. Awasthi S, Cheng J, Singhal SS, Saini MK, Pandya U, Pikula S, Bandorowicz-Pikula J, Singh SV, Zimniak P, Awasthi YC. Novel function of human RLIP76: ATP-dependent transport of glutathione conjugates and doxorubicin. Biochemistry 2000;39:9327–9334
23. Awasthi S, Singhal SS, Sharma R, Zimniak P, Awasthi YC. Transport of glutathione conjugates and chemotherapeutic drugs by RLIP76 (RALBP1): a novel link between G-protein and tyrosine kinase signaling and drug resistance. Int J Cancer 2003;106:635–646
24. Rossé C, L'Hoste S, Offner N, Picard A, Camonis J. RLIP76, an effector of the Ral GTPases, is a platform for Cdk1 to phosphorylate epsin during the switch off of endocytosis in mitosis. J Biol Chem 2003;278:30597–30604
25. Singhal SS, Yadav S, Roth C, Singhal J. RLIP76: a novel glutathione-conjugate and multi-drug ransporter. Biochem Pharmacol 2009;77:761–769
26. Singhal SS, Yadav S, Singhal J, Sahu M, Sehrawat A, Awasthi S. Diminished drug transport and augmented radiation sensitivity caused by loss of RLIP76. FEBS Lett 2008;582:3408–3414
27. Awasthi S, Singhal SS, Yadav S, Singhal J, Drake K, Nadkar A, Zajac E, Wickramarachchi D, Rowe N, Yacoub A, Boor P, Dwivedi S, Dent P, Jarman WE, John B, Awasthi YC. RLIP76 is a major determinant of radiation sensitivity. Cancer Res 2005;65:6022–6028
28. Kim JK, Fillmore JJ, Sunshine MJ, Albrecht B, Higashimori T, Kim DW, Liu ZX, Soos TJ, Cline GW, O'Brien WR, Littman DR, Shulman GI. PKC-theta knockout mice are protected from fat-induced insulin resistance. J Clin Invest 2004;114:823–827
29. Opie LH, Newsholme EA. The inhibition of skeletal-muscle fructose 1,6-diphosphatase by adenosine monophosphate. Biochem J 1967;104:353–360
30. Taketa K, Pogell BM. Allosteric inhibition of rat liver fructose 1,6-diphosphatase by adenosine 5′-monophosphate. J Biol Chem 1965;240:651–662
31. Gierow P, Jergil B. A spectrophotometric method for the determination of glucose-6-phosphatase activity. Anal Biochem 1980;101:305–309
32. Gryczynski Z, Gryczynski I, Lakowicz JR. Basics of fluorescence and FRET. In *Molecular Imaging: FRET Microscopy and Spectroscopy*. Periasami A, Day RN (Eds.). Oxford, U.K., Oxford Unversity Press, 2005, p. 21–56
33. Singhal J, Singhal SS, Yadav S, Suzuki S, Warnke MM, Yacoub A, Dent P, Bae S, Sharma R, Awasthi YC, Armstrong DW, Awasthi S. RLIP76 in defense of radiation poisoning. Int J Rad Oncol Biol Phys 2008;72:553–561
34. Warnke MM, Wanigasekara E, Singhal SS, Singhal J, Awasthi S, Armstrong DW. The determination of glutathione-4-hydroxynonenal (GSHNE), E-4-hydroxynonenal (HNE), and E-1-hydroxynon-2-en-4-one (HNO) in mouse liver tissue by LC-ESI-MS. Anal Bioanal Chem 2008;392:1325–1333
35. Rossé C, Hatzoglou A, Parrini MC, White MA, Chavrier P, Camonis J. RalB mobilizes the exocyst to drive cell migration. Mol Cell Biol 2006;26:727–734
36. Singhal SS, Yadav S, Drake K, Singhal J, Awasthi S. Hsf-1 and POB1 induce drug sensitivity and apoptosis by inhibiting Ralbp1. J Biol Chem 2008;283:19714–19729
37. Katz A, Nambi SS, Mather K, Baron AD, Follmann DA, Sullivan G, Quon MJ. Quantitative insulin sensitivity check index: a simple, accurate method for assessing insulin sensitivity in humans. J Clin Endocrinol Metab 2000;85:2402–2410
38. Matthews DR, Hosker JP, Rudenski AS, Naylor BA, Treacher DF, Turner RC. Homeostasis model assessment: insulin resistance and beta-cell function from fasting plasma glucose and insulin concentrations in man. Diabetologia 1985;28:412–419
39. Singhal SS, Awasthi S. Glutathione-conjugate transport and stress-response signaling: role of RLIP76. In *Toxicology of Glutathione S-Transferases*. Awasthi YC, Ed. Boca Raton, FL, CRC Press, 2006, p. 231–256
40. Kurucz I, Morva A, Vaag A, Eriksson KF, Huang X, Groop L, Koranyi L. Decreased expression of heat shock protein 72 in skeletal muscle of patients with type 2 diabetes correlates with insulin resistance. Diabetes 2002;51:1102–1109
41. Yamashita R, Kikuchi T, Mori Y, Aoki K, Kaburagi Y, Yasuda K, Sekihara H. Aldosterone stimulates gene expression of hepatic gluconeogenic enzymes through the glucocorticoid receptor in a manner independent of the protein kinase B cascade. Endocr J 2004;51:243–251
42. Andrews RC, Walker BR. Glucocorticoids and insulin resistance: old hormones, new targets. Clin Sci (Lond) 1999;96:513–523